Title

Rearrangements of the Chrysanthenol Core: Application to a Formal Synthesis of Xishacorene B

Journal

Journal of the American Chemical Society, 143(48)

ISSN

0002-7863

Authors

Jones, Kerry E
Park, Bohyun
Doering, Nicolle A
et al.

Publication Date

2021-12-08

DOI

10.1021/jacs.1c10804

Peer reviewed

Published in final edited form as:

J Am Chem Soc. 2021 December 08; 143(48): 20482–20490. doi:10.1021/jacs.1c10804.

Rearrangements of the Chrysanthenol Core: Application to a Formal Synthesis of Xishacorene B

Kerry E. Jones,
Department of Chemistry, University of California, Berkeley, California 94720, United States

Bohyun Park,
Department of Chemistry, Korea Advanced Institute of Science and Technology (KAIST), Daejeon 34141, Korea;

Center for Catalytic Hydrocarbon Functionalizations, Institute for Basic Science (IBS), Daejeon 34141, Korea;

Nicolle A. Doering,
Department of Chemistry, University of California, Berkeley, California 94720, United States

Mu-Hyun Baik,
Department of Chemistry, Korea Advanced Institute of Science and Technology (KAIST), Daejeon 34141, Korea;

Center for Catalytic Hydrocarbon Functionalizations, Institute for Basic Science (IBS), Daejeon 34141, Korea;

Richmond Sarpong
Department of Chemistry, University of California, Berkeley, California 94720, United States;

Abstract

Reported here are substrate-dictated rearrangements of chrysanthenol derivatives prepared from verbenone to access complex bicyclic frameworks. These rearrangements set the stage for a 10-step formal synthesis of the natural product xishacorene B. Key steps include an anionic allenol oxy-Cope rearrangement and a Suárez directed C–H functionalization. The success of this work was guided by extensive computational calculations which provided invaluable insight into the reactivity of the chrysanthenol-derived systems, especially in the key oxy-Cope rearrangement.

Corresponding Authors: Mu-Hyun Baik – Department of Chemistry, Korea Advanced Institute of Science and Technology (KAIST), Daejeon 34141, Korea; Center for Catalytic Hydrocarbon Functionalizations, Institute for Basic Science (IBS), Daejeon 34141, Korea; mbaik2805@kaist.ac.kr, **Richmond Sarpong** – Department of Chemistry, University of California, Berkeley, California 94720, United States; rsarpong@berkeley.edu.

Supporting Information

The Supporting Information is available free of charge at https://pubs.acs.org/doi/10.1021/jacs.1c10804.
Experimental procedures, characterization data, and spectra for all new compounds, as well as crystallographic data and Cartesian coordinates of DFT-optimized structures and computational details (PDF)

Accession Codes

CCDC 2108926, 2108934, and 2108936 contain the supplementary crystallographic data for this paper. These data can be obtained free of charge via www.ccdc.cam.ac.uk/data_request/cif, or by emailing data_request@ccdc.cam.ac.uk, or by contacting The Cambridge Crystallographic Data Centre, 12 Union Road, Cambridge CB2 1EZ, UK; fax: +44 1223 336033.

Complete contact information is available at: https://pubs.acs.org/10.1021/jacs.1c10804

The authors declare no competing financial interest.

Graphical Abstract

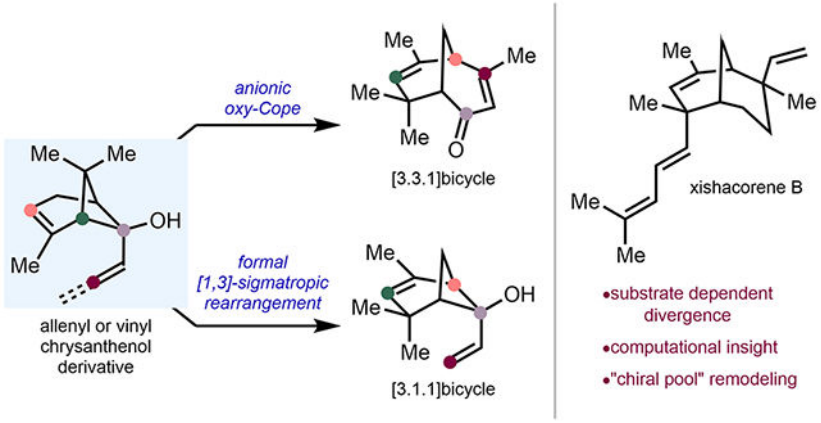

INTRODUCTION

The “chiral pool” has long served as a starting point for the synthesis of complex molecules, including natural products.[1–5] “Chiral pool” compounds (e.g., terpenoids **1** and **8**, Figure 1) are naturally available, enantioenriched, small molecules that possess functional handles for diversification. However, the terpenoid “chiral pool” is limited in the variety of carbocyclic scaffolds that it encompasses. Many researchers have sought to overcome this shortcoming by leveraging functional groups inherent to “chiral pool” compounds to skeletally remodel the carbon backbone and gain access to a broader array of novel structures. As outlined by Maimone and co-workers,[5] total syntheses that originate from “chiral pool” terpenoids are influenced by three major factors: the availability of the starting materials, advances in chemical synthesis methodology that can be implemented, as well as, of course, creativity in the synthesis strategy that is adopted. Overall, the discovery of novel strategies that remodel the core framework of the “chiral pool” should significantly expand the available starting inputs for total synthesis and facilitate access to unique chemical space with greater ease and efficiency.

Our research group has had a longstanding interest in utilizing carvone (**1**) as a starting material to access highly functionalized cyclohexenones through a key cyclobutanol intermediate and C–C bond cleavage strategy. This approach has been successfully applied toward the total syntheses of the phomactins,[6,7] longiborneol terpenoids,[8] preparation of the taxane core,[9] as well as the total synthesis of xishacorene B[10] (**2**, Figure 1). In our previously reported synthesis of **2**, transition-metal-mediated C–C bond cleavage/cross-coupling of a cyclobutanol precursor (**3**) was employed to afford highly functionalized monocyclic precursor **4** (Figure 1B). Cyclization of **4** elaborated it to a bicyclo[3.3.1]nonane framework, which afforded xishacorene B (**2**)—a total of 10 steps from (*R*)-carvone (**1**).[10]

As we sought to expand this “chiral pool” remodeling strategy beyond carvone (**1**), we again selected the xishacorenes as a proving ground. Xishacorenes A–C (**5**, **2**, **6**) were isolated in 2017 from *Sinularia polydactula*, a soft coral found off the coast of the Xisha Islands in China.[11] These hydrocarbon natural products contain a bicyclo[3.3.1]nonane skeleton with

an appended diene side chain, differing in stereochemistry about C-13 and the position of unsaturation at C-10, C-11, and C-12 (Figure 1B). This class of compounds is believed to arise biosynthetically from an acid-mediated cyclization of fuscol (**7**), which our group leveraged in a bioinspired total synthesis of xishacorene congeners, including a related compound that we named xishacorene D.[12] Although the parent natural products do not possess notable bioactivity (presumably due to their highly hydrophobic nature), oxidized derivatives have been shown to be inhibitors of interferon regulatory factor (IRF).[12]

By coupling robust strategies in C–H functionalization[13] with "chiral pool" remodeling, we recognized that the xishacorenes could be prepared from pinene derivatives—specifically verbenone (**8**). This orthogonal strategy to the xishacorenes would highlight the utility of "chiral pool" bicyclic terpenoids. Importantly, C–H functionalization would provide access to functional handles not inherent in the starting material, expanding our scope of synthetically viable compounds. On the basis of this strategy, we envisioned preparing xishacorene B (**2**) from (*S*)-verbenone (**8**), as illustrated in Figure 1C. Retrosynthetically, xishacorene B (**2**) could arise from ketone **9**, which possesses the desired oxygenation to direct C–H functionalization of one of the geminal methyl groups to install the diene side chain of the xishacorenes. Ketone **9** could arise from [3.1.1]bicycle **10V** through an anionic oxy-Cope rearrangement[14,15] in the forward sense, followed by β-functionalization. [3.1.1]Bicycle **10V** could be accessed from chrysanthenone (**11**), which can be prepared from commercially available (*S*)-verbenone (**8**).

RESULTS AND DISCUSSION

Rearrangement Studies.

Our studies commenced with a known photomediated rearrangement of (*S*)-verbenone (**8**) to chrysanthenone (**11**) through a Norrish Type I process (Scheme 1).[16,17] In our initial investigations, addition of vinyl magnesium bromide to chrysanthenone (**11**) afforded the desired alcohol (**10V**) required for the planned [3,3]-sigmatropic (oxy-Cope) rearrangement in moderate yield along with an unexpected rearranged [3.1.1]bicycle, **12V**, which presumably arises from a formal [1,3]-sigmatropic rearrangement. Bicycle **12V** was unambiguously characterized by X-ray crystallographic analysis. We observed that the yields of **10V** and **12V** differed on the basis of the reaction duration: over prolonged reaction times, **12V** was obtained as the major product. This observation suggested that **12V** likely arose from **10V** through a formal [1,3]-alkyl shift.

We also investigated formation of an alkynyl chrysanthenol derivative that could serve as an alternative oxy-Cope precursor and would ultimately install unsaturation between C-1 and C-6 of the resulting [3.3.1]bicycle, setting the stage for C-1 functionalization en route to the xishacorenes (see **9**, Figure 1c). Treating chrysanthenone (**11**) with propynyl magnesium bromide gave **10P** as the sole product (i.e., without the competing formal 1,3-alkyl shift) regardless of the reaction duration or temperature. This product was also unambiguously characterized by X-ray crystallographic analysis.

The differences in the propensity for chrysanthenol scaffolds such as **10V** and **10P** to rearrange under the reaction conditions is unusual. We sought to gain more insight into

the origin of this differing reactivity by preparing and screening various chrysanthenol derivatives. These were synthesized by adding a variety of Grignard reagents (alkenyl-, alkynyl-, aryl-, and alkyl-based) to chrysanthenone (**11**) at selected temperatures and quenching excess Grignard reagent at selected time points, as illustrated in Table 1.

All of the adducts resulting from addition of alkenyl Grignard reagents (entries 1–3) underwent rearrangement to the isomeric formal 1,3-alkyl migration adduct (see **12**, Table 1). In these cases, prolonged reaction times and higher reaction temperatures led to an increase in the amount of **12**. However, the extent of rearrangement observed had a strong dependence on the alkenyl Grignard nucleophile.

Interestingly, when an *E*/*Z* mixture of the 1-propenyl Grignard reagent was used (entry 2), the rearranged product (**12Pr**) bearing exclusively the *E* olefin group was isolated following prolonged reaction at room temperature, along with the chrysanthenol derivative (**10Pr**) bearing both *E*- and *Z*-disposed olefins. On the other hand, heating the same reaction mixture to higher temperatures (50 °C for 17 h) resulted in formation of the rearranged isomer (**12Pr**) as a mixture of *E* and *Z* olefins. This temperature-dependent outcome suggested that the steric demand posed by the *E*- or *Z*-disposed substituent affected the rate of rearrangement, with the *E* double bond isomer rearranging more readily at room temperature. The combined ratio of *E* and *Z* olefins was maintained in all cases, indicating there was no *E*/*Z* isomerization occurring throughout the reaction.

While the alkenyl adducts displayed a rearrangement reactivity trend consistent with substitution on the alkene group, alkynyl adducts (entries 4 and 5), aryl adducts (entries 6 and 7), as well as alkyl adducts (entries 8 and 9) did not undergo any observable rearrangement under any of the reaction conditions.

To provide support for the proposal that the rearrangement occurred following 1,2-addition of the alkenyl Grignard reagents to chrysanthenone (**11**), vinyl 1,2-adduct (**10V**) was subjected to the reaction conditions. A mixture of starting material **10V** as well as rearranged alcohol **12V**, albeit in diminished yields, was obtained (Figure 2A), consistent with the trend observed in Table 1. Under the reaction conditions, rearranged vinyl alcohol **12V** remained unchanged (Figure 2B). To determine if this rearrangement would occur on the free alcohol (i.e., not the magnesium alkoxide), neutral alcohol **10V** was heated in a sealed vial at 150 °C. The rearranged alcohol (**12V**) was observed in 19% yield—produced along with several volatile compounds that were not characterized (Figure 2C). To gain insight into the underlying mechanism of this transformation, we have undertaken in-depth computational studies.

Computational Insights into the Observed Rearrangement Reaction.

Quantum mechanical calculations using density functional theory (DFT) were conducted, and the most salient results are summarized in Figure 3. For each case that was analyzed, our calculations were initiated with the magnesium alkoxide dimer of the 1,2-adduct, which is assumed to be the most stable intermediate under the reaction conditions on the basis of the Schlenk equilibrium.[18] Vinyl adduct **10′V** was selected as a representative model. As described above, while the [3,3]-sigmatropic rearrangement to yield **13′V** was anticipated,

it was not observed experimentally. Rather, a formal [1,3]-sigmatropic rearrangement of **10′V** occurred. As shown in Figure 3, the barrier for the anionic oxy-Cope rearrangement (**10′V-TSc**) was calculated to be 22.2 kcal/mol, which is 4.2 kcal/mol higher than the barrier of the homolytic C–C bond cleavage (**10′V-TS**) associated with a formal [1,3]-sigmatropic rearrangement. These barrier differences are consistent with the experimental observations and suggest that the [1,3]-sigma-tropic rearrangement is ~5 orders of magnitude faster than the anionic oxy-Cope rearrangement. Therefore, we focused our attention on the C–C bond homolysis leading to the bicyclo[3.1.1] product, as illustrated (solid black line in Figure 3).

Given that the magnesium alkoxide was more likely to exist than the corresponding alcohol under the reaction conditions, we also considered an alternative, heterolytic C–C bond breaking process, with the associated transition state ^{CS}**10′V-TS** (blue dotted line in Figure 3). This alternative reaction pathway leads to the ring-opened intermediate ^{CS}**14′V**, which was calculated to be 6.1 kcal/mol lower in free energy than rearranged product **12′V**. However, the barrier was found to be non-competitive at 22.8 kcal/mol, which is 4.7 kcal/mol higher than the homolytic cleavage from **10′V**. Therefore, we propose that the [1,3]-sigmatropic rearrangement proceeds through homolytic C–C bond cleavage to afford open-shell singlet intermediate **14′V** at 4.7 kcal/mol with an associated barrier of only 18.0 kcal/mol.

Having established a plausible reaction mechanism for the formal [1,3]-sigmatropic rearrangement, we sought to better understand the factors that affect the rate of the rearrangement. These analyses were conducted using the neutral intermediates **10** and **14** (Figure 4) in order to reduce potential artifacts associated with the computational treatment of the Schlenk equilibrium intermediates, which we have found difficult to model computationally. Although the formal [1,3]-sigmatropic rearrangement of the neutral alcohol only proceeds at higher temperatures experimentally, we believe that the computational modeling of this simpler substrate will capture the key features of the reaction. Experimentally, none of the products arising from an oxy-Cope rearrangement were observed for the neutral alcohol or magnesium alkoxide of the vinyl adduct.

As the formal [1,3]-sigmatropic rearrangement involves homolytic C–C bond breaking, the energies of the open-shell singlet intermediates such as **14′V** or **14** are key to the rate constant for C–C bond cleavage. Employing the Bell–Evans–Polanyi principle,[19] we hypothesized that the barrier heights are directly proportional to the enthalpy difference (ΔH) of the open-shell singlet intermediates prepared from the addition of different nucleophiles to chrysanthenone (**11**, Figure 4A). Accordingly, we investigated the ΔH between various 1,2-addition products (**10**) and their corresponding C–C bond-cleaved open-shell singlet intermediates (**14**). Specifically, we analyzed vinyl- (**10V**), allenyl- (**10A**), propynyl- (**10P**), *p*-methoxyphenyl- (**10Ph**), and methylchrysanthenol (**10M**) adducts as representative examples (Figure 4A). In good agreement with our experimental observations, **10V** has the lowest ΔH value of 13.7 kcal/mol (Figure 4D), whereas **10A**, **10P**, **10Ph**, and **10M** show notably higher enthalpies of 17.2, 19.1, 20.5, and 25.6 kcal/mol, respectively.

Because the only difference among the substrates that were examined is the exocyclic radical functionality in the diradical intermediate, the differences in ΔH should be governed

by the relative stability of the corresponding radicals formed upon homolytic C–C bond cleavage. To determine the effect of the substituents on the radical intermediates, the radical stabilization energies (RSEs)[20] of the exocyclic radicals were calculated using the following isodesmic reaction

$$\mathbf{14H} + \bullet CH_3 \rightarrow \mathbf{14} + CH_4, \qquad \Delta H_{rxn} \tag{1}$$

where **14H** represents **14** bearing a hydrogen at C-6 (Figure 4b). Our calculations showed that the diradical bearing a vinyl group (**14V**) is most stable with a RSE of −29.1 kcal/mol, whereas **14M** is the least stable with a RSE of −16.2 kcal/mol, as enumerated in Figure 4D. Notably, the increase in RSE in comparing the vinyl-bearing diradical intermediate to the methyl-bearing diradical reveals a quantitative trend that mirrors the increase in ΔH. This correlation between the ΔH and RSE supports our assertion that the change of ΔH arises from the relative stability of the exocyclic radicals in the diradical intermediates for each adduct.

Finally, we conducted intrinsic bond orbital (IBO)[21,22] analysis along the intrinsic reaction coordinate (IRC) of the C–C bond cleavage step to obtain a more quantitative depiction of how the covalent electron pair homolyzes to form the diradical intermediate. Figure 4C depicts energy levels of the two orbitals from the breaking of the C1–C6 bond to yield the exocyclic radical ($E(\alpha)$, shown in yellow) and endocyclic radical ($E(\beta)$, shown in blue), respectively. For each of the chrysanthenol derivatives, the energy levels of the endocyclic allylic radicals $E(\beta)$ were calculated to be very similar (−7.13 to −6.96 eV when $S^2 \approx 1$ (**14**); Figure 4D). However, the energy levels of the exocyclic radicals ($E(\alpha)$) varied substantially. Note that for **10V** the exocyclic allylic radical is 0.47 eV lower in energy than the endocyclic allylic radical as a result of the adjacent alkoxide moiety. In the case of **14V** and **14A**, $E(\alpha)$ was calculated to be −7.59 and −7.37 eV, respectively, whereas, for **14P** and **14Ph**, the energies of the propargylic and benzylic radicals were calculated to be −7.30 and −7.15 eV, respectively. Furthermore, **14M** has an $E(\alpha)$ value of −6.59 eV. Therefore, the relative energy of the exocyclic radical on the hydroxy-bearing π system plays a key role in determining the overall barrier for the C–C bond homolysis, whereas the endocyclic allylic radical does not play a significant role.

Formal Synthesis of Xishacorene B.

With [3,3]-sigmatropic rearrangement precursors **10V** and **10P** in hand, we attempted both oxy-Cope and anionic oxy-Cope rearrangements. In both cases, the only observed rearrangement was to [3.1.1]bicycle **12V** in the vinyl case (Figure 2C), or nonspecific decomposition of the starting material. Given numerous emerging studies of the unusual reactivity of allenol-bearing substrates compared to their vinyl analogues,[23,24] we sought to examine the reactivity of the allenyl adduct of chrysanthenol (**10A**, Figure 4) under conditions that would generate the magnesium alkoxide, as outlined in Figure 2. The calculations described above suggested that the energy for C–C bond homolysis of **10A** would lie between that of the vinyl and alkynyl chrysanthenol adducts (**10V** and **10P**, respectively). To validate our computations, the allenyl chrysanthenol adduct (**10A**) was synthesized as described below.

Subjecting chrysanthenone (**11**) to the *in situ*-generated Grignard reagent of tetrahydropyran-protected propargyl alcohol (**15**) provided alkyne adduct **16** (Scheme 2). Alternatively, **16** was formed in one step from (*S*)-verbenone (**8**) by direct addition of the alkynyl Grignard reagent to the reaction mixture following irradiation in cyclohexane (see the Supporting Information for details). Alkyne **16** was subsequently converted to allenyl chrysanthenol **10A** by treatment with $LiAlH_4$. Upon reaction of allenol **10A** with ethylmagnesium bromide (to form the magnesium alkoxide), the rearranged [3.1.1]bicycle arising from formal [1,3]-sigmatropic rearrangement was anticipated to form. However, under these conditions, [3.3.1]bicycle **13A** was produced as the major product through a formal [3,3]-sigmatropic rearrangement followed by isomerization to the enone. A detailed mechanistic analysis of this remarkable switch in selectivity is discussed in the next section. Following optimization, it was determined that heating alkyne **16** in the presence of $LiAlH_4$, ethylmagnesium bromide, and 1,4-cyclohexadiene afforded [3.3.1]bicycle **13A** directly—presumably through an *in situ* generated allene and subsequent [3,3]-sigmatropic rearrangement.

Following our synthesis of the bicyclo[3.3.1] framework of the xishacorenes, we focused on peripheral functionalization to access natural products in this family. Conjugate addition of a vinyl group was achieved with vinyl cuprate to give ketone **9**. C–H functionalization of the geminal methyl substituents was investigated next. From the ketone oxidation state, we investigated Sanford's oxime-directed C–H oxidation.[25,26] However, this approach did not result in functionalization on either of the geminal methyl groups. Our analysis suggests that the ketone group (and therefore the corresponding oxime) likely bisects the geminal methyl groups, which does not allow for the productive conformation for an oxime-directed C–H functionalization. We posited that, by reducing the ketone to the corresponding α-disposed hydroxy group, we could establish a more favorable conformation to functionalize one of the geminal methyl groups. We found that both dissolving metal reduction (Li^0, NH_3) and hydride reduction (with $LiAlH_4$) proceeded with the same sense of diastereoselectivity, giving rise to alcohol **17**. A Suárez reaction[27] successfully functionalized the axially disposed methyl group to afford ether **18**, which was unambiguously characterized by X-ray crystallography.

To complete the synthesis of xishacorene B (**2**), we attempted ionic reductions of the tetrahydrofuran ring (Et_3SiH/TFA, $Et_3SiH/B(Ar_F)_3$) of **18** to afford the primary alcohol and directly intercept our previous synthesis of the natural product. However, we observed either only recovered starting material (i.e., **18**) or reduction at the less substituted methylene position of the tetrahydrofuran to return secondary alcohol **17**. Unfortunately, standard ether cleavage conditions (TMSI, BBr_3) did not afford any ring-opened products and resulted in either recovered **18** or nonspecific decomposition. However, employing conditions disclosed by Shin and co-workers (AcCl, Fe^0)[28] for the opening of tetrahydrofuran rings gave secondary chloride **19** in moderate yield. The chloride substituent could provide a functional handle for diversification of this intermediate to C-5 derivatized analogues of the xishacorenes. However, for the purposes of the synthesis of the natural product, radical dehalogenation followed by acetate cleavage afforded primary alcohol **20**, a known intermediate from our previous synthesis of xishacorene B (**2**). As previously reported,

xishacorene B (**2**) can be prepared from alcohol **20** by installing the diene side chain in a two-step sequence.[10] The route reported here constitutes a complementary approach to xishacorene B (**2**) in a total of 10 steps from commercially available (*S*)-verbenone (**8**).

Computational Insight into the Reactivity of Allenyl Chrysanthenol 10A.

To better understand the unique reactivity of allenyl chrysanthenol substrate **10′A**, computational studies were undertaken. Unlike the vinyl or alkynyl chrysanthenol adducts, allenyl substrate **10′A** underwent formal oxy-Cope rearrangement to give the [3.3.1]bicyclic product **13′A**. Calculated reaction energy profiles for the anionic oxy-Cope rearrangement and homolytic C–C bond cleavage of **10′A** are illustrated in Figure 5A, showing barriers of 19.2 and 19.8 kcal/mol, respectively. Compared to the vinyl chrysanthenol adduct (**10′V**), the barrier for the C–C bond cleavage is 1.9 kcal/mol higher for **10′A**. This computed value is in good agreement with the rationale discussed above; Figure 4D shows a ΔH value of 18.8 kcal/mol for **10A**, which is 3.5 kcal/mol higher than that for **10V**.

Despite the relative energies of the associated intermediates and transition states, the anionic oxy-Cope rearrangement of **10′A** has a barrier that is 3.0 kcal/mol lower than that for **10′V**, which is rationalized by considering the relative energies of the reactant and the product. For the vinyl-substituted case, the free energy difference (ΔG) between the magnesium alkoxide of vinyl adduct **10′V** and the immediate product of anionic oxy-Cope rearrangement, enolate **13′V**, was calculated to be 33.8 kcal/mol (Figure 3). On the other hand, the analogous product for the allenyl case, dienolate **13′A**, is 52.1 kcal/mol more stable than **10′A**. On the basis of the Hammond postulate,[29] the related transition state, **10′A-TSc**, should be earlier and have a lower barrier. Figure 5B depicts the two transition states, **10′V-TSc** and **10′A-TSc**, associated with the anionic oxy-Cope rearrangements of **10′V** and **10′A**, respectively. In **10′A-TSc**, the length of the breaking C1–C6 bond was calculated to be 2.21 Å, which is 0.24 Å shorter than what was found in **10′V-TSc** (Figure 5B), consistent with an earlier transition state.

This difference between the reactivity of the vinyl- and allenyl-bearing substrates can be rationalized on the basis of the electronic properties of the allenyl moiety. Both **10′A-TSc** and **10′V-TSc** have much higher associated barriers than conventional anionic oxy-Cope rearrangements (Figure 5A)[30] due to the distortion required to achieve the optimal transition state geometry. As illustrated in Figure 6A, C-12 must rotate ~90° and break the exocyclic π bond to form the C3–C12 bond. Therefore, **10′V** does not experience a simple suprafacial–suprafacial interaction but rather requires additional energy to break the π bond. As a result, the two allyls in **10′V-TSc** do not possess effective orbital overlap, which leads to a weak interaction and relatively long interatomic distances (2.45, 2.73 Å, Figure 5B). Furthermore, the relatively small HOMO–LUMO gap of 2.76 eV (Figure 6C) and the large HOMO energy change of 1.54 eV from **10′V** toward **10′V-TSc** (Figure 6C) render this transition a higher energy process.

On the other hand, for the allenyl system, significant rotation is not required, since the p-orbital (shown in red, Figure 6B) is productively oriented for C3–C12 bond formation. The p-orbital at the terminal methylene, depicted in red in Figure 6B, rotates by 90° into

conjugation with the orthogonal π bond, shown in blue. Consequently, there is less of an energetic penalty associated with the distortion of **10′A-TSc** and, in addition, the two allyl fragments here experience better orbital overlap; compare the larger HOMO–LUMO gap of 3.68 eV in **10′A-TSc** (Figure 6D) and the smaller HOMO energy change of 1.10 eV (from **10′A** toward **10′A-TSc**) to **10′V-TSc**. Overall, these differences lead to an accessible oxy-Cope rearrangement with smaller interatomic distances in the transition state (2.21 Å, 2.49 Å, Figure 5B) for **10′A**. More detailed MO diagrams are presented in the Supporting Information.

CONCLUSION

Using a combination of a “chiral pool” remodeling strategy and C–H functionalization, we have achieved a formal synthesis of xishacorene B from commercially available (*S*)-verbenone in 10 steps. During the course of our synthetic studies, we encountered several rearrangements of chrysanthenol derivatives that proceeded with unusual selectivity. We gained insight into the nature of these processes using computational studies, which, in turn, provided a foundation for many of the successes that were realized in this work. For example, through key computational insights, our understanding of the differing reactivity of vinyl- and allenyl-bearing chrysanthenol derivatives in a planned anionic oxy-Cope rearrangement set the stage for the preparation of the bicyclo[3.3.1] core of the xishacorenes. From (*S*)-verbenone, the overall transformation from [3.1.1]-bicycle to [3.3.1]bicycle was achieved through an initial photomediated rearrangement and a key anionic oxy-Cope rearrangement of an allenyl-substituted chrysanthenol derivative. Peripheral functionalization of a gem-dimethyl group in the [3.3.1]bicycle using a Suárez C–H oxygenation sets the stage for the preparation of xishacorene B. This route demonstrates the combined power of structural remodeling and directed C–H functionalization to access complex scaffolds in short order.

Supplementary Material

Refer to Web version on PubMed Central for supplementary material.

ACKNOWLEDGMENTS

R.S. is grateful to the National Institutes of General Medical Sciences (R35 GM130345) and the NSF Center for Computer Assisted Synthesis (CCAS; CHE-1925607) for financial support. N.A.D. thanks the NSF GRFP for a graduate fellowship (DGE 1106400). The computational studies were supported financially by the Institute for Basic Science in Korea (IBS-R10-A1). We thank Dr. Hasan Celik, Dr. Alicia Lund, and UC Berkeley’s NMR facility in the College of Chemistry (CoC-NMR) for spectroscopic assistance. Instruments in the CoC-NMR are supported in part by NIH S10OD024998. We also thank Dr. Nicholas Settineri (UC Berkeley) for single-crystal X-ray diffraction studies and Dr. Miao Zhang (DOE Catalysis Facility, UC Berkeley) for support with the acquisition of IR data. We thank Mr. Gyumin Kang and Mr. Joon Heo (KAIST) for fruitful discussions.

REFERENCES

(1). Gaich T; Mulzer J In Comprehensive Chirality; Carreira EM, Yamamoto H, Eds.; Elsevier Ltd.: 2012; Vol. 2, pp 163–206.

(2). Money T; Wong MKC The Use of Cyclic Monoterpenoids as Enantiopure Starting Materials in Natural Product Synthesis. Stud. Nat. Prod. Chem 1995, 16, 123–288.

(3). Ho T-L Enantioselective Synthesis: Natural Products from Chiral Terpenes; Wiley: 1992.

(4). Nugent WA; RajanBabu TV; Burk MJ Beyond Nature's Chiral Pool: Enantioselective Catalysis in Industry. Science 1993, 259, 479–483. [PubMed: 17734166]

(5). Brill ZG; Condakes ML; Ting CP; Maimone TJ Navigating the Chiral Pool in the Total Synthesis of Complex Terpene Natural Products. Chem. Rev 2017, 117, 11753–11795. [PubMed: 28293944]

(6). Kuroda Y; Nicacio KJ; Alves da Silva I Jr.; Leger PR; Chang S; Gubiani JR; Deflon VM; Nagashima N; Rode A; Blackford K; Ferreira AG; Sette LD; Williams DE; Andersen RJ; Jancar S; Berlinck RGS; Sarpong R Isolation, synthesis and bioactivity studies of phomactin terpenoids. Nat. Chem 2018, 10, 938–945. [PubMed: 30061613]

(7). Leger PR; Kuroda Y; Chang S; Jurczyk J; Sarpong R C–C Bond Cleavage Approach to Complex Terpenoids: Development of a Unified Total Synthesis of the Phomactins. J. Am. Chem. Soc 2020, 142, 15536–15547. [PubMed: 32799452]

(8). Lusi RF; Sennari G; Sarpong R Total Synthesis of Nine Longiborneol Sesquiterpenoids Using a Functionalized Camphor Strategy. ChemRxiv, June 14, 2021, ver. 1. DOI: 10.26434/chemrxiv.14774919.v1.

(9). Weber M; Owens K; Masarwa A; Sarpong R Construction of Enantiopure Taxoid and Natural Product-like Scaffolds Using a C–C Bond Cleavage/Arylation Reaction. Org. Lett 2015, 17, 5432–5435. [PubMed: 26485318]

(10). Kerschgens I; Rovira AR; Sarpong R Total Synthesis of (−)-Xishacorene B from (*R*)-Carvone Using a C–C Activation Strategy. J. Am. Chem. Soc 2018, 140, 9810–9813. [PubMed: 30032603]

(11). Ye F; Zhu Z-D; Chen J-S; Li J; Gu Y-C; Zhu W-L; Li X-W; Guo Y-W Xishacorenes A–C, Diterpenes with Bicyclo[3.3.1]-nonane Nucleus from the Xisha Soft Coral *Sinularia polydactyla*. Org. Lett 2017, 19, 4183–4186. [PubMed: 28762746]

(12). Rovira AR; Müller N; Deng W; Ndubaku C; Sarpong R Bio-inspired synthesis of xishacorenes A, B, and C, and a new congener from fuscol. Chem. Sci 2019, 10, 7788–7791. [PubMed: 31588327]

(13). Abrams DJ; Provencher PA; Sorensen EJ Recent applications of C–H functionalization in complex natural product synthesis. Chem. Soc. Rev 2018, 47, 8925–8957. [PubMed: 30426998]

(14). Berson JA; Jones M Jr. Synthesis of ketones by the thermal isomerization of 3-hydroxy-1,5-hexadienes. The oxy-Cope rearrangement. J. Am. Chem. Soc 1964, 86, 5019–5020.

(15). Evans DA; Golob AM [3,3]Sigmatropic rearrangements of 1,5-diene alkoxides. Powerful accelerating effects of the alkoxide substituent. J. Am. Chem. Soc 1975, 97, 4765–4766.

(16). Hurst JJ; Whitham GH The Photochemistry of Verbenone. J. Chem. Soc 1960, 2864–2869.

(17). Erman WF Photochemical transformation of unsaturated bicyclic ketones. Verbenone and its photodynamic products of ultraviolet irradiation. J. Am. Chem. Soc 1967, 89, 3828–3841.

(18). Peltzer RM; Eisenstein O; Nova A; Cascella M How Solvent Dynamics Controls the Schlenk Equilibrium of Grignard Reagents: A Computational Study of CH_3MgCl in Tetrahydrofuran. J. Phys. Chem. B 2017, 121, 4226–4237. [PubMed: 28358509]

(19). Evans MG; Polanyi M Further Considerations on the Thermodynamics of Chemical Equilibria and Reaction Rates. Trans. Faraday Soc 1936, 32, 1333–1360.

(20). Firestone RA Applications of the Linnett Electronic Theory to Organic Chemistry. Part III. Linnett Structures for 1,3-Dipoles and for the Diradical Intermediates in 1,3-Dipolar Cycloadditions. J. Chem. Soc. A 1970, 1570–1575.

(21). Knizia G Intrinsic Atomic Orbitals: An Unbiased Bridge between Quantum Theory and Chemical Concepts. J. Chem. Theory Comput 2013, 9, 4834–4843. [PubMed: 26583402]

(22). Knizia G; Klein JEMN Electron Flow in Reaction Mechanisms—Revealed from First Principles. Angew. Chem., Int. Ed 2015, 54, 5518–5522.

(23). Seiser T; Cramer N Rhodium(I)-Catalyzed Enantioselective Activation of Cyclobutanols: Formation of Cyclohexane Derivatives with Quaternary Stereogenic Centers. Chem. - Eur. J 2010, 16, 3383–3391. [PubMed: 20146275]

(24). Wu P; Ma S Halogen-Substituted Allenyl Ketones through Ring Opening of Nonstrained Cycloalkanols. Org. Lett 2021, 23, 2533–2537. [PubMed: 33733787]

(25). Desai LV; Hull KL; Sanford MS Palladium-Catalyzed Oxygenation of Unactivated sp^3 C–H Bonds. J. Am. Chem. Soc 2004, 126, 9542–9543. [PubMed: 15291549]

(26). Neufeldt SR; Sanford MS O-Acetyl Oximes as Transformable Directing Groups for Pd-Catalyzed C–H Bond Functionalization. Org. Lett 2010, 12, 532–535. [PubMed: 20041702]

(27). Concepción JI; Francisco CG; Hernández R; Salazar JA; Suárez E Intramolecular hydrogen abstraction. Iodosobenzene diacetate, an efficient and convenient reagent for alkoxy radical generation. Tetrahedron Lett. 1984, 25, 1953–1956.

(28). Bodduri VDV; Choi K-M; Vaidya RR; Patil K; Chirumarry S; Jang K; Yoon Y-J; Falck JR; Shin D-S An efficient iron catalyzed regioselective acylative cleavage of ethers: scope and mechanism. Tetrahedron Lett. 2015, 56, 7089–7093.

(29). Hammond GS A Correlation of Reaction Rates. J. Am. Chem. Soc 1955, 77, 334–338.

(30). Haeffner F; Houk KN; Reddy YR; Paquette LA Mechanistic Variations and Rate Effects of Alkoxy and Thioalkoxy Substituents on Anionic Oxy-Cope Rearrangements. J. Am. Chem. Soc 1999, 121, 11880–11884.

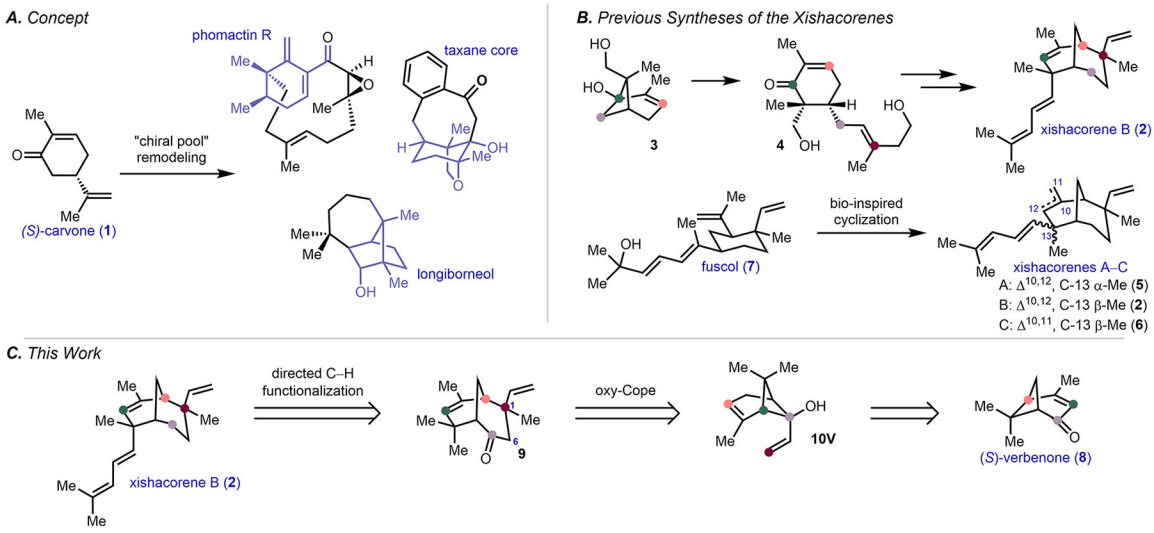

Figure 1.

(A) Examples of natural product scaffolds previously prepared in the Sarpong group using a carvone remodeling strategy. (B) Previous syntheses of the xishacorenes. (C) A newly planned retrosynthesis of xishacorene B (**2**) from (*S*)-verbenone (**8**).

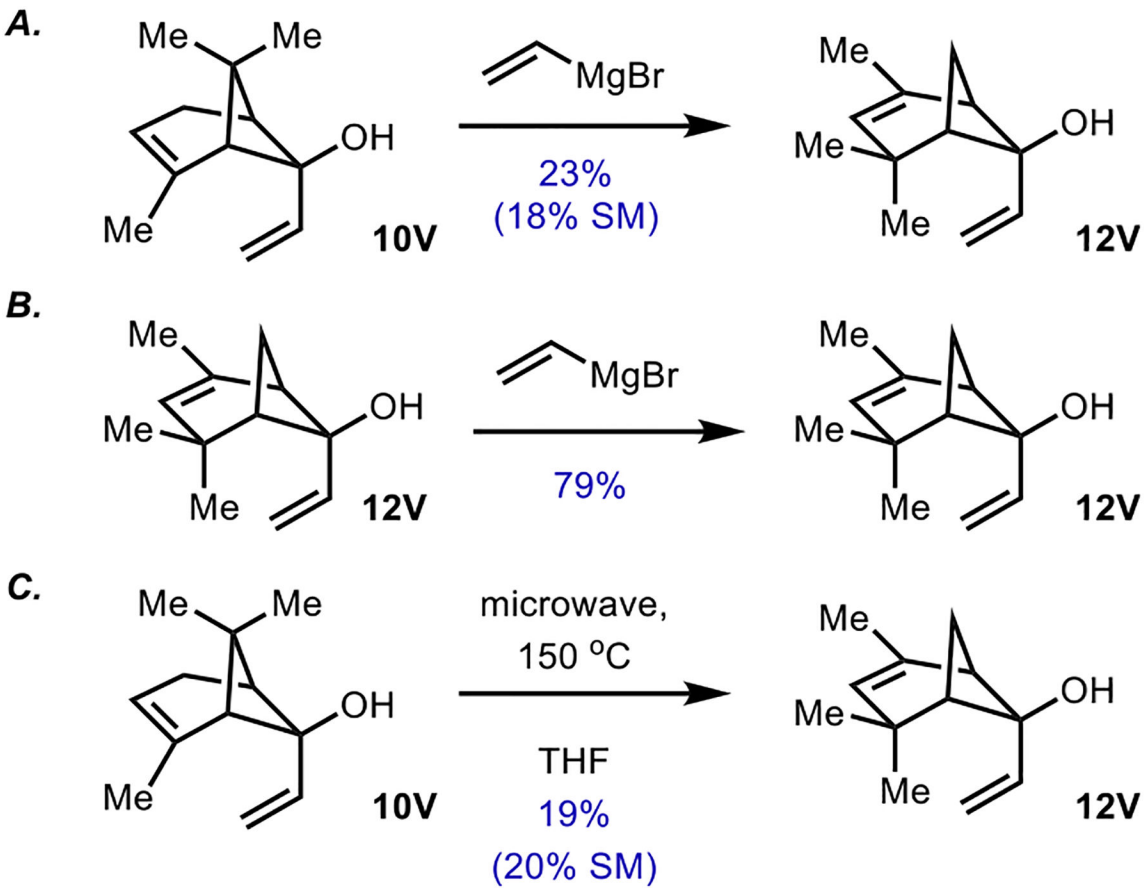

Figure 2.
Control reactions for the rearrangement of vinyl chrysanthenol **10V**.

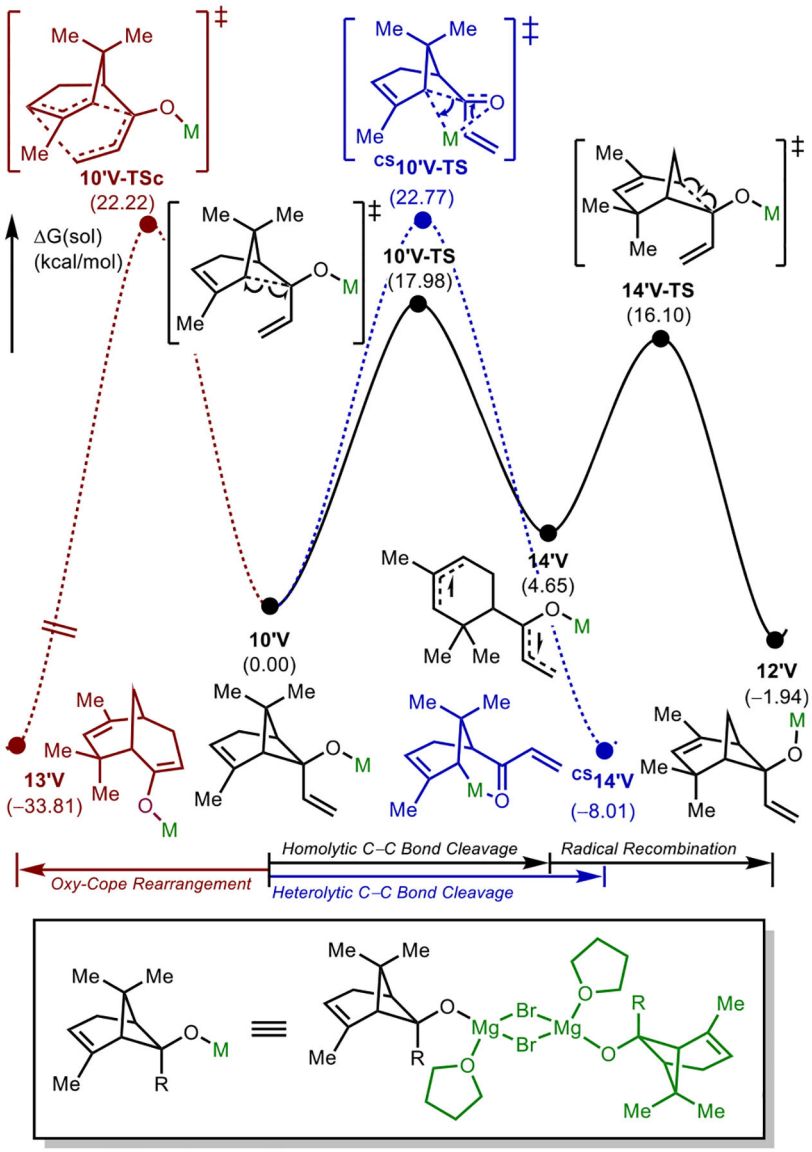

Figure 3.

Free energy profile of plausible reaction pathways. The black trace represents the homolytic C–C bond cleavage and the blue dotted trace represents the heterolytic C–C bond cleavage. The red dotted line represents the oxy-Cope rearrangement. Geometry optimization and vibration energy calculations were conducted using DFT with the B3LYP-D3/6–31G** (LANL2DZ for Br) functional and basis set. Single-point energies were re-evaluated by the B3LYP-D3/6–311+ +G** (SDD for Br) level of theory in conjunction with a continuum solvation model using ε = 7.4257 for THF.

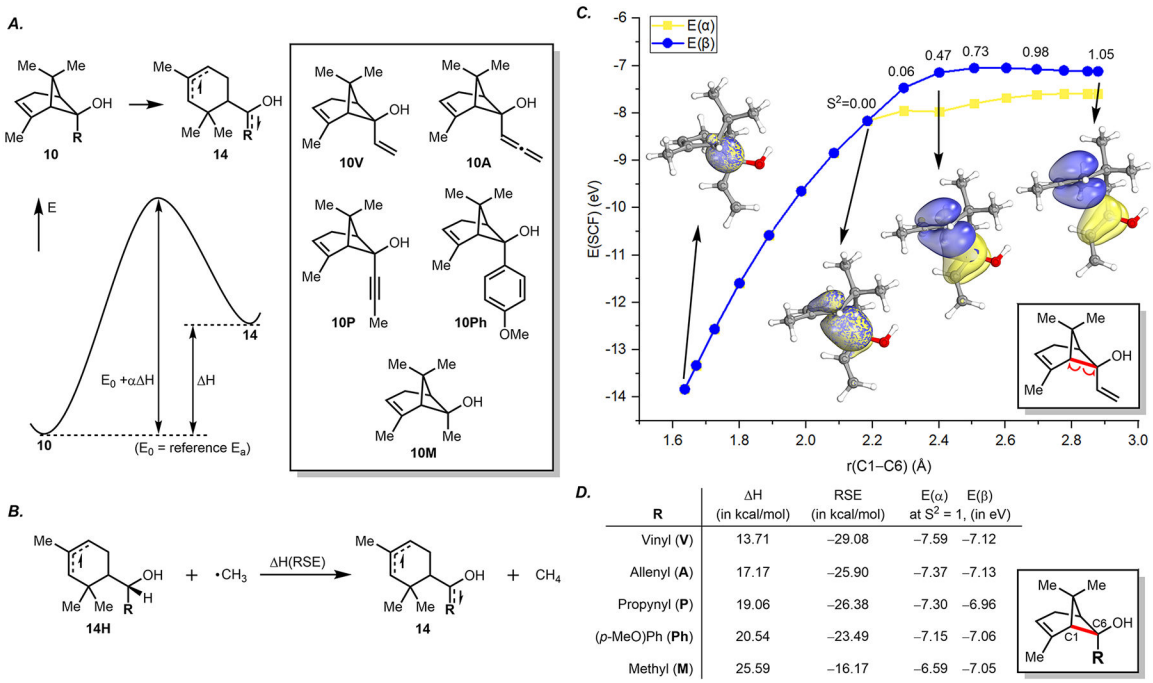

R	ΔH (in kcal/mol)	RSE (in kcal/mol)	E(α) at S^2 = 1, (in eV)	E(β)
Vinyl (**V**)	13.71	–29.08	–7.59	–7.12
Allenyl (**A**)	17.17	–25.90	–7.37	–7.13
Propynyl (**P**)	19.06	–26.38	–7.30	–6.96
(*p*-MeO)Ph (**Ph**)	20.54	–23.49	–7.15	–7.06
Methyl (**M**)	25.59	–16.17	–6.59	–7.05

Figure 4.

(A) Homolytic C–C bond cleavage of chrysanthenol derivatives to compare the relative barriers using the Bell–Evans–Polanyi principle. (B) The reaction scheme for the calculation of the radical stabilization energy (RSE). (C) Intrinsic bond orbital (IBO) profile of **10V** along the intrinsic reaction coordinate for the formation of the diradical (**10V** → **14V**). $E(\alpha)$ and $E(\beta)$ represent the energies of the two radicals associated with the diradical intermediate. (D) Computed ΔH, RSE, $E(\alpha)$, and $E(\beta)$ values depending on the functional groups, **R**. Orbital energies were re-evaluated by the IBO exponent 2 orbital localization method based on the DFT calculation results using the B3LYP-D3/def2TZVP level of theory.

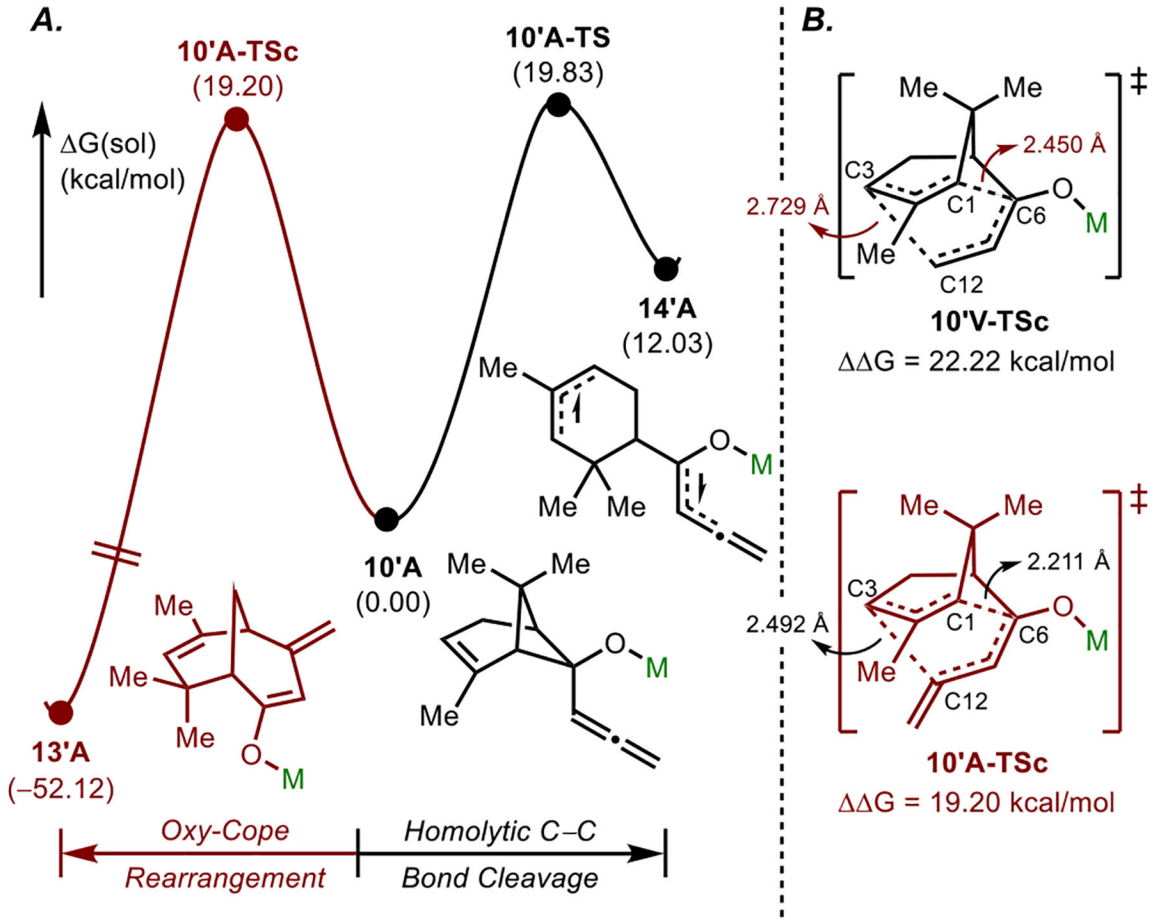

Figure 5.

(A) Free energy profile of the oxy-Cope rearrangement (red trace) and the homolytic C–C bond cleavage (black trace) of the allenyl substrate **10′A**. (B) Transition state descriptions and FMO energy levels for **10′V-TSc** and **10′A-TSc**.

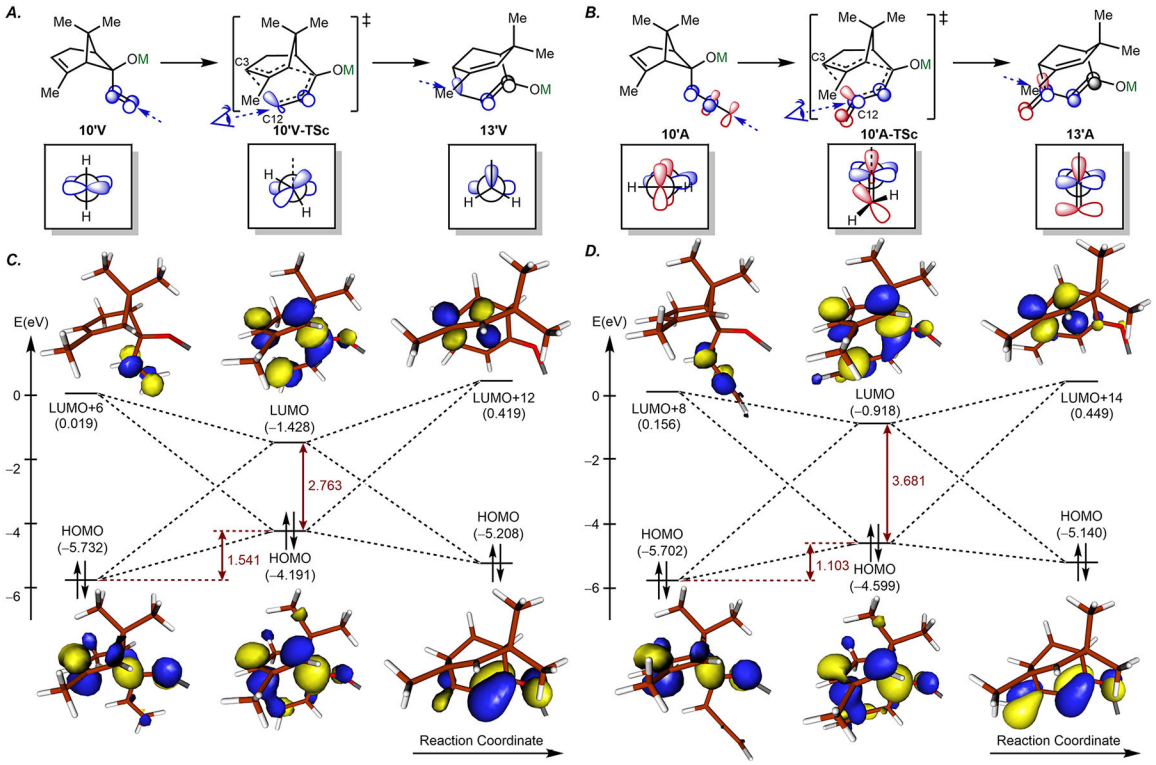

Figure 6.

(A, B) Reaction schemes and Newman projections of the oxy-Cope rearrangements of **10′V** and **10′A**. (C, D) FMO diagrams of parts A and B along the reaction coordinate. Unnecessary fragments which have no contribution to FMOs are omitted for clarity. Isodensity value = 0.05 au.

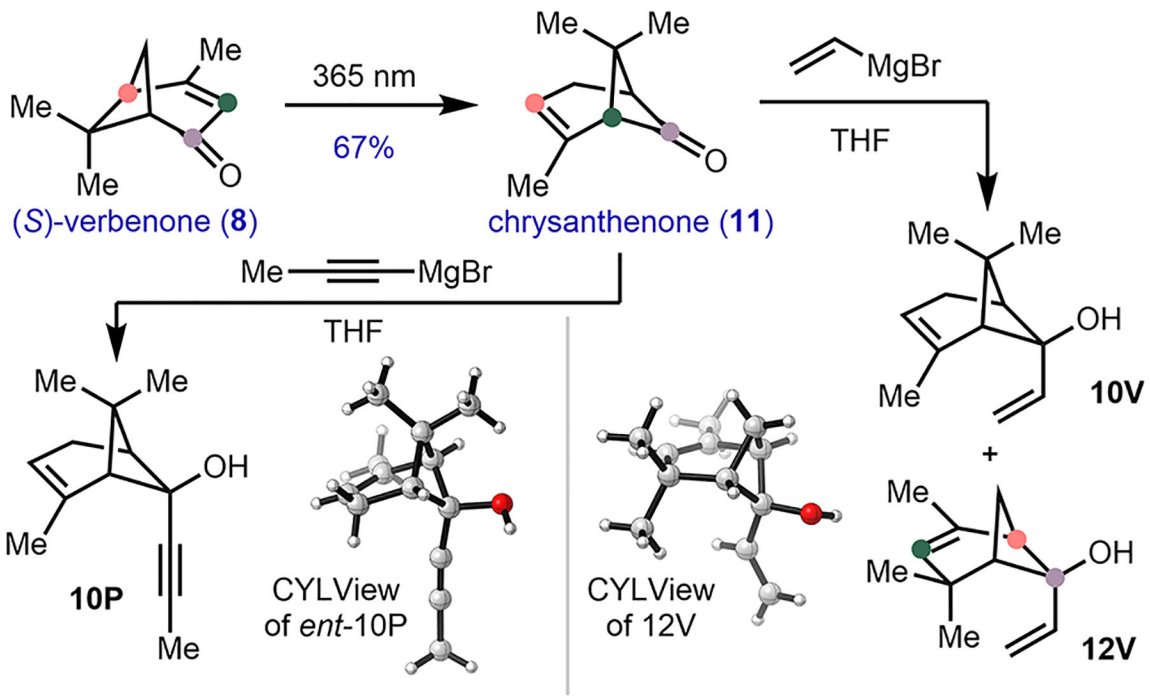

Scheme 1.

Formation of Chrysanthenol Derivatives (10V and 10P) and Rearranged [3.1.1]Bicycle (12V) from (*S*)-Verbenone (8)

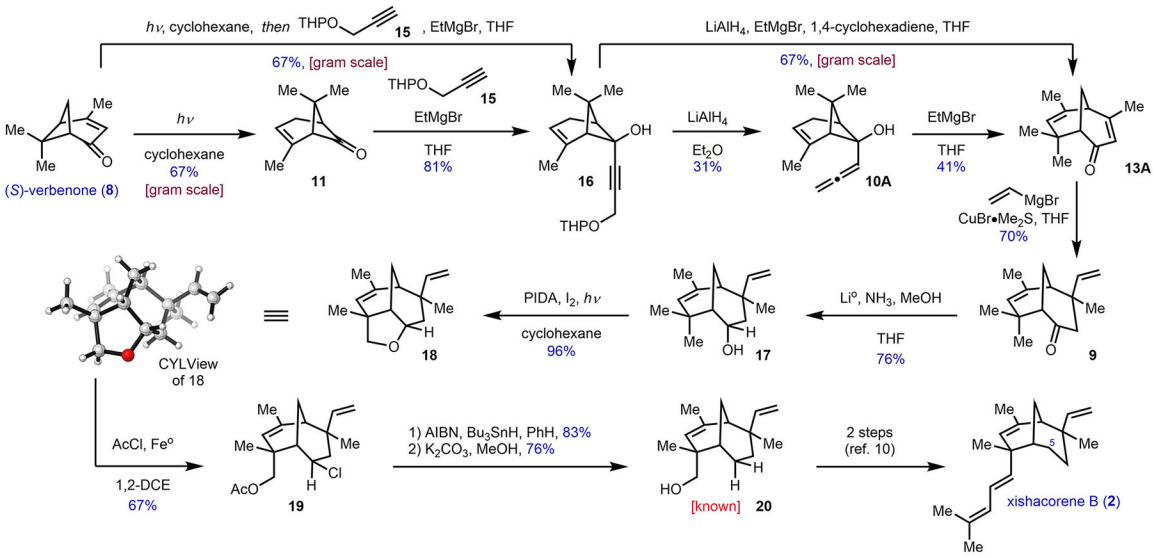

Scheme 2.
Formal Synthesis of Xishacorene B (2)

Table 1.

Reaction of Selected Grignard Reagents with Chrysanthenone (11)[a]

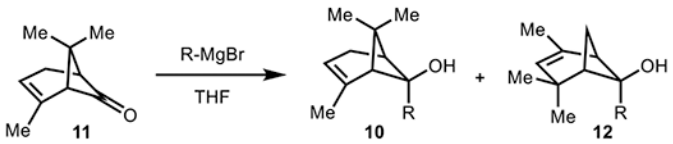

entry		1	2	3	4	5	6	7	8	9
R=				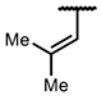			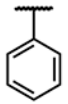	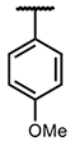		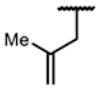
	yield 11	0%	33%	23%	71%	15%	0%	0%	38%	0%
25 °C, 3 h	**yield 10**	30%	46%*	69%	14%	70%	95%	96%	22%	78%
	yield 12	31%	9%	0%	0%	0%	0%	0%	0%	0%
	yield 11	0%	31%	22%	39%	0%	0%	0%	7%	0%
25 °C, 17 h	**yield 10**	0%	41%*	71%	48%	77%	96%	79%	50%	61%
	yield 12	40%	16%	3%	0%	0%	0%	0%	0%	0%
	yield 11	0%	6%	9%	0%	0%	0%	0%	0%	0%
50 °C, 17 h	**yield 10**	0%	0%	39%	47%	70%	96%	00%	65%	66%
	yield 12	53%	48%*	25%	0%	0%	0%	0%	0%	0%

[a]Reactions were conducted with 0.1 mmol of chrysanthenone (**11**) and 2 equiv of RMgBr in THF to give a final concentration of 0.2 M. Yields determined by ^{1}H NMR with ethylene carbonate as the internal standard.

*Combined yield of *E*/*Z* olefins.